Indian Journal of Pure & Applied Physics
Vol. 51, November 2013, pp. 769-779

Dielectric behaviour, ionic conductivity and structure of high energy ball mill blended melt pressed and solution cast solid polymeric nanocomposite electrolytes

Shobhna Choudhary[1], Adam Bald[2] & R J Sengwa[1]*

[1]Dielectric Research Laboratory, Department of Physics, J N V University, Jodhpur 342 005, India

[2]Department of Physical Chemistry of Solutions, University of Łódź, 90-236 Łódź, Pomorska 163, Poland

*E-mail: rjsengwa@rediffmail.com

Received 17 May 2013; revised 20 July 2013; accepted 12 September 2013

The high energy ball mill blended solid polymeric nanocomposite electrolytes (SPNEs) comprising poly(ethylene oxide) (PEO), lithium perchlorate ($LiClO_4$) and montmorillonite (MMT) clay as nanofiller (PEO_{20}-$LiClO_4$–*x* wt% MMT; where EO:Li^+ = 20:1, and *x* = 0, 1, 2, 3 and 5) were prepared by melt pressing and solution casting techniques. The complex dielectric function, *ac* ionic conductivity, electric modulus and impedance spectra of these SPNE films have been investigated by dielectric relaxation spectroscopy in the frequency range 20 Hz – 1 MHz at ambient temperature. The values of dielectric relaxation strength, relaxation time of Li^+ cation coordinated PEO segmental motion and *dc* ionic conductivity have been determined and their correlations with ion transportation in these materials have been explored. Results reveal that the *dc* ionic conductivity of solution cast SPNE films has gradual increase with loading of MMT concentration up to 5 wt%. In case of melt pressed SPNE films, the *dc* ionic conductivity shows anomalous variation with MMT concentration and it is maximum at 1 wt% MMT. The X-ray diffraction study of these SPNE films confirms the formation of ion-dipolar complexes between the ether oxygen atoms of PEO chain, the lithium cations and the siloxane groups of MMT nano-platelets. The d_{001}-spacing of intercalated MMT, crystallite size of PEO and the relative changes in PEO peaks intensity with MMT concentration have been evaluated from the XRD patterns. These XRD parameters were discussed in relation to the MMT intercalated structures and amorphicity of the electrolyte materials. The correlation between ionic conductivity and the structural properties of these electrolytes has also been explored.

Keywords: Polymer nanocomposite electrolyte, Dielectric property, Ionic conductivity, XRD, High energy ball milling

1 Introduction

Due to light weight, leak proof, flexible in nature, compact in size, suitable life span, and easy in preparation, a tremendous work is in progress on the ion conducting solid polymeric electrolytes (SPEs) and also the inorganic nano materials filled solid polymeric nanocomposite electrolytes [1–33] (SPNEs). These materials are in demand for the growing technologies in the area of separators and electrolytes, which are used in design and fabrications of ion conduction based electrochromic and energy storage devices.

The ionic conductivity of SPEs and SPNEs depends on the types of polymer, alkali salt, inorganic nanofiller and also the plasticizer used in their synthesis. The ceramic and other nanofillers alter the amorphous phase of polymer, degree of salt dissociation, ion conduction paths, the dynamics of cation coordinated polymer segmental motion and the ion-pairing effect, due to which the ionic conductivity of the SPNEs materials shows a significant increase as compared to the SPEs materials. The nanofillers also improve the mechanical and thermal properties of the SPNEs materials. Most of these solid electrolyte materials have low ionic conductivity at ambient temperature and below it, which limit their use in technical applications. To overcome this drawback, the synthesis of SPNE materials with a state-of-the-art is very important as far as the enhancement of ionic conduction is concerned.

Solution casting technique is the most common procedure used for the synthesis of SPEs and SPNEs. Besides this, now-a-days melt pressed technique has become very popular due to solvent free and rapid processing of the material[6,29–36]. Further, it has been revealed that the mechanical and electromagnetic treatments during the synthesizing process of SPNEs are highly effective for the increase of their ionic conductivity[7,25,37]. The mechanical blending of the electrolyte composition using high energy ball milling is an effective way to moderate the ion conduction paths in solid polymeric electrolyte[38–41]. Recent

studies on the SPNEs revealed that the ball milling for long duration induces the amorphicity of the electrolyte due to chain scission and fracture of polymer powder, and also improve the blending of active and inactive phases of the nanocomposite, which prolonged their ionic conductivity[38,39,41]. The synthesis of SPNEs by long duration of ball mill blending results the enhancement of ionic conductivity by one order of magnitude which is mainly due to polymer molecular weight loss and it is not tolerable. The chain scission and fracture of polymer reduce the physico-chemical properties of the SPNE materials, which is similar to the plasticized electrolytes, although they have high ionic conductivity. Keeping short duration of ball milling, the loss of polymer molecular weight and degradation of its mechanical properties can be prevented, which is very important for the high stability of electrolyte material.

Considering the above facts, poly(ethylene oxide) (PEO), lithium perchlorate ($LiClO_4$) and montmorillonite (MMT) clay as inorganic nanofiller were initially blended for short duration using high energy ball mill and their SPNEs films were prepared by melt pressed and solution casting techniques. The detailed electrical and ion conduction behaviour of these films has been studied by dielectric relaxation spectroscopy at ambient temperature. Among the nanofillers, montmorillonite (MMT) clay is widely used as inorganic nanofiller for the enhancement of ionic conductivity, and also the mechanical and thermal properties of the SPNEs materials[4,7,8,27,29-32]. Therefore, it is used for the synthesis of SPNE materials in the present investigation. The hydrophilic MMT clay is also called inorganic polymer, which is 2:1 phyllosilicate and chemically it is a metal silicate. Its nanometer thick layered sheets are stacked by weak dipolar or van der Waals forces, and have both surface and edge charges. In water and various organic polar solvents, the MMT clay has excellent swelling properties owing to the intercalation (absorption) of solvent molecules in the clay galleries and their adsorption on its external surfaces.

2 Experimental Details

2.1 Preparation of electrolyte films

The PEO of molecular weight 600,000 g/mol, $LiClO_4$ (dry battery grade) and hydrophilic MMT (Nanoclay, PGV, a product of Nanocor®), were purchased from Sigma-Aldrich, USA. Acetonitrile of spectroscopic grade was purchased from Loba Chemie, India.

For the preparation of PEO_{20}-$LiClO_4$–*x* wt% MMT electrolyte films by melt pressed (MP) technique, firstly, the appropriate amount of PEO and $LiClO_4$ were mixed in 20:1 molar ratio of the monomer units (EO) of PEO to the Li^+ cations of $LiClO_4$. The required amounts of MMT were added in the respective composition of PEO_{20}-$LiClO_4$ for 0, 1, 2, 3 and 5 wt% MMT concentration with respect to the weight of PEO. Further, each composition was homogeneously mixed using agate mortar and pestle. After that each composition was blended by high energy planetary ball mill (Retsch PM 100) in agate vessel with agate balls at 200 rpm for 10 m. The balls and the electrolyte composition weight ratio was kept 22:1. The MP films of these ball milled PEO_{20}-$LiClO_4$–*x* wt% MMT compositions were synthesized by melt pressing under 2 tons of pressure per unit area at 80°C (above the PEO melting temperature ~65°C) in 60 mm diameter stainless steel die with a suitable spacer using hot polymer press film making unit.

For the synthesis of ball milled solution cast (SC) electrolyte films of PEO_{20}-$LiClO_4$–*x* wt% MMT, initially the required amount of PEO, $LiClO_4$ and MMT for 0, 1, 2, 3 and 5 wt% MMT concentration were dissolved/swelled in acetonitrile for 24 h, and then the each viscous electrolyte solution was ball milled for 10 m duration at 200 rpm. After that these solutions were cast onto the polypropylene petri dishes and allowed to dry at room temperature. Finally, the free standing SPNEs films were vacuum dried at 40°C for 24 h.

2.2 Measurements

Agilent technologies 4284A precision LCR meter and the 16451B solid dielectric test fixture (active electrodes diameter 38 mm) were used for measurements of capacitance C_p, parallel resistance R_p and loss tangent (dissipation factor) tanδ of the electrolyte films in the frequency range from 20 Hz to 1 MHz at ambient temperature (27±1°C). The expression used for evaluation of complex dielectric function $\varepsilon^*(\omega)=\varepsilon' - j\varepsilon''$, alternating current (*ac*) electrical conductivity $\sigma^*(\omega) = \sigma' + j\sigma''$, electric modulus $M^*(\omega) = M' + jM''$ and complex impedance $Z^*(\omega) = Z' - jZ''$ of these SPNEs films are described elsewhere[29,42]. These complex quantities are alternative representation of same macroscopic relaxation data and can be transformed to each other

according to the scheme; $1/\varepsilon^*(\omega) = j\omega C_0 Z^*(\omega) = M^*(\omega) = j\omega\varepsilon_0/\sigma^*(\omega)$, where angular frequency $\omega = 2\pi f$, f is linear frequency, C_0 is capacity of dielectric test fixture without electrolyte film and ε_0 is permittivity in vacuum.

The X-ray diffraction (XRD) patterns of these SPNEs films and the powder samples of MMT and $LiClO_4$ were recorded using PANalytical X′pert Pro MPD diffractometer of Cu Kα radiation (1.5406 Å) operated at 45 kV and 40 mA with a scanned step size of 0.05° and 1 s duration. The powder samples were tightly filled in the sample holder whereas the films were placed on top of the sample holder for recording their XRD patterns in the 2θ range 3.8°-30° at room temperature. The values of crystalline peaks position, their intensities (number of counts) and full width at half maximum (FWHM) were determined using PANalytical X'pert HighScore® software.

3 Results and Discussion

3.1 Structural analysis

The XRD patterns of MMT, $LiClO_4$, solution cast pure PEO film, and ball milled synthesized solution cast (SC) films of PEO_{20}-$LiClO_4$–x wt% MMT electrolytes are shown in Fig. 1. The XRD patterns of melt pressed pure PEO and ball mill blended melt pressed (MP) films of PEO_{20}–$LiClO_4$–x wt% MMT electrolytes are shown in Fig. 2. The major diffraction peaks of the PEO crystalline phase were observed at 2θ ~19° and ~23° corresponding to crystal reflections 120 and concerted 112,032, respectively, for both the SC and MP synthesized pure PEO films, which are in agreement with the earlier results[4,43]. The XRD pattern of MMT powder has 001 peak at 2θ = 7.028° (Fig. 1), whereas a peak in this pattern at 2θ = 19.79° can be related to the impurities (mostly quartz and feldspar) present in the MMT, and it shows good resemblance of XRD pattern of the bentonite clay[44]. Similarly, the intense peaks observed in XRD pattern of $LiClO_4$ at 2θ = 21.02° and 23.04° are also found to be good agreement with its earlier investigations[45].

Significant changes in intensity profile of 001 peak of MMT (inset of Figs 1 and 2), and also the 120 and 112,032 peaks of PEO in the PEO_{20}-$LiClO_4$–x wt% MMT electrolyte films were observed with their preparation techniques and the MMT concentrations. The values of Bragg's angle 2θ and d_{001} basal spacing of 001 peak of MMT for the electrolytes are determined and recorded in Table 1. These values reveal the formation of intercalated MMT structures beside their exfoliation in the electrolytes, and the intercalation spacing (d_{001}) initially has an increase up to 3 wt% MMT and then it decreases at 5 wt% (Table 1). The MMT concentration dependent d_{001}

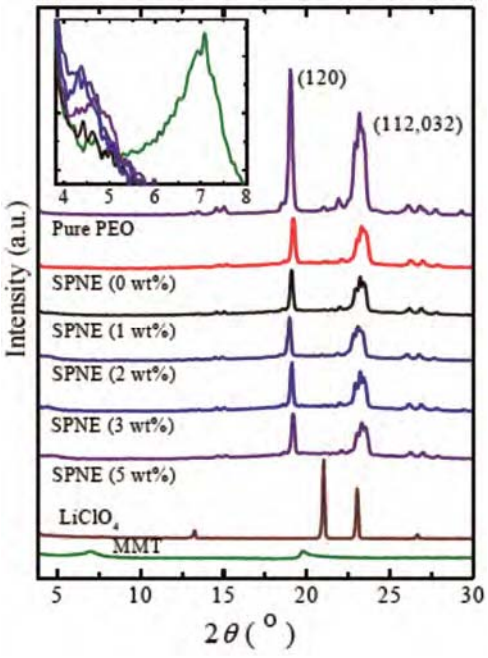

Fig. 1 — XRD patterns of MMT powder, $LiClO_4$ powder, solution cast synthesized pure PEO and ball mill blended PEO_{20}–$LiClO_4$–x wt% MMT electrolyte films. Inset shows the enlarged view of small angle XRD patterns

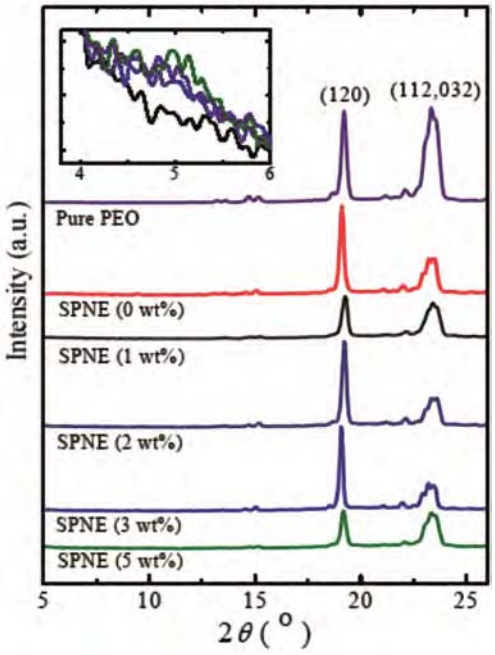

Fig. 2 — XRD patterns of melt pressed synthesized pure PEO and ball mill blended PEO_{20}-$LiClO_4$–x wt% MMT electrolyte films. Inset shows the enlarged view of small angle XRD patterns

Table 1 — Values of Bragg's angle 2θ, MMT basal spacing d_{001}, full width at half maximum FWHM, crystallite size L and crystalline peak intensity (counts) I corresponding to MMT 001 reflection of ball mill blended solution cast and melt pressed PEO_{20}-$LiClO_4$–x wt% MMT electrolyte films.

x wt% MMT	2θ (°)	d_{001} (nm)	FWHM×10^3 (rad)	L (nm)	I (Counts)
Pure MMT	7.028	1.257	17.1	8.44	520
Solution cast electrolytes					
1	5.02	1.759	1.0	151.01	14
2	4.69	1.883	8.2	17.59	84
3	4.41	2.002	11.3	12.85	112
5	4.71	1.875	11.6	12.51	126
Melt pressed electrolytes					
1	5.35	1.651	3.0	48.29	27
2	5.09	1.735	3.0	48.29	46
3	4.87	1.813	3.4	43.03	52
5	5.02	1.759	10.3	14.08	67

values infer that there are dramatic changes of ion-dipolar interactions in these electrolytes which results in the irregular variation of d_{001} spacing at low MMT concentration. It has been observed that the d_{001} spacing of the SC films is high as compared to the MP films of these electrolytes at same MMT concentration (Table 1). It is expected because there is large probability of the hydrophilic polymer intercalation in swelled MMT galleries in the solutions, and this is also favoured by high intensity values I (counts) of 001 peak for SC films (except 1 wt% MMT). A very low intensity at 1 wt% MMT electrolyte film inferred the existence of large amount of MMT in exfoliated form at this concentration. The values of Bragg's angle 2θ of PEO main crystalline peaks (120 and 112,032) and the corresponding (d-spacing d_{120} and d_{112}), the FWHM (β) (the broadening of peak at half-height expressed in radians of 2θ i.e. width measured in 2θ degrees and then multiplied by $\pi/180$), mean crystallite length L, peak intensity I(I_{PEO} or I_{SPNE}) and the percentage relative intensity RI of crystalline peaks (I_{SPNE}/ I_{PEO}) of the SC and MP electrolyte films are determined from their XRD patterns and these are presented in Tables 2 and 3, respectively. The d-spacing between diffractional lattice planes of intercalated MMT and the PEO was determined by Bragg's relation $\lambda = 2d \sin\theta$, whereas the mean crystallite size (length) L in the direction perpendicular to hkl plane of PEO was evaluated by Scherrer's equation $L = 0.94\lambda/\beta\cos\theta$.

Tables 2 and 3 indicate that the changes in 2θ values of 120 or 112,032 crystalline peaks of PEO and also corresponding d_{120} or d_{112} values are found

Table 2 — Values of Bragg's angle 2θ, PEO basal spacing d, full width at half maximum FWHM, crystallite size L, crystalline peak intensity I and percent relative intensity ratio RI (I_{SPNE}/I_{PEO}) at 120 and 112,032 reflection peaks of solution cast synthesized pure PEO and ball mill blended solution cast (SC) PEO_{20}-$LiClO_4$–x wt% MMT electrolyte films

x wt% MMT	2θ (°)	d (nm)	FWHM×10^3 (rad)	L (nm)	I (counts)	RI (%)
Parameters of 120 reflection peak						
Pure PEO	19.03	0.466	4.38	33.52	15296	100.00
0	19.20	0.462	4.21	34.92	4975	32.52
1	19.09	0.465	3.65	40.26	4472	29.24
2	18.97	0.467	3.91	37.56	4413	28.85
3	19.11	0.464	3.18	46.23	4450	29.09
5	19.19	0.462	3.60	40.85	4205	27.49
Parameters of 112,032 reflection peak						
Pure PEO	23.22	0.383	13.23	11.18	9515	100.00
0	23.40	0.380	13.02	11.36	3631	38.16
1	23.22	0.383	8.85	16.71	3569	37.51
2	23.14	0.384	13.11	11.28	2936	30.86
3	23.22	0.383	6.42	23.02	3630	38.15
5	23.32	0.381	12.85	11.51	3261	34.27

Table 3 — Values of Bragg's angle 2θ, PEO basal spacing d, full width at half maximum FWHM, crystallite size L, crystalline peak intensity I and percent relative intensity ratio RI (I_{SPNE}/I_{PEO}) at 120 and 112,032 reflection peaks of melt pressed pure PEO and ball mill blended melt pressed (MP) PEO_{20}-$LiClO_4$–x wt% MMT electrolyte films

x wt% MMT	2θ (°)	d (nm)	FWHM×10^3 (rad)	L (nm)	I (counts)	RI (%)
Parameters of 120 reflection peak						
Pure PEO	19.22	0.461	4.70	31.28	12964	100.00
0	19.12	0.464	4.05	36.27	12416	95.77
1	19.27	0.460	5.39	27.24	5968	46.04
2	19.23	0.461	4.17	35.21	12240	94.42
3	19.09	0.465	3.37	43.60	11802	91.04
5	19.20	0.462	4.82	30.49	5236	40.39
Parameters of 112,032 reflection peak						
Pure PEO	23.41	0.380	13.13	11.27	12569	100.00
0	23.37	0.380	12.29	12.04	4802	38.21
1	23.47	0.379	12.74	11.61	4558	36.26
2	23.48	0.379	12.39	11.94	3765	29.95
3	23.22	0.383	12.69	11.65	3478	27.67
5	23.41	0.380	13.11	11.28	4654	37.03

insignificant with the method of preparation and the MMT concentrations of the investigated SPNE films. But the significant variation in the values of FWHM, L and RI reveals that the complexations behaviour and amorphous phase of the composition comprising PEO, $LiClO_4$ and MMT vary with their synthesization route and also the MMT concentrations, because the RI values have the direct correlation with degree of crystallinity of the polymer composites[44,46]. The comparative L values of SC and MP electrolyte films

with pure PEO (Tables 2 and 3) inferred that there is enhancement of crystallite size due to complexations in most of the electrolytes. But the decrease in intensity of the 120 and 112,032 peaks of these electrolytes and their corresponding *RI* values suggest the suppression of crystalline phase of PEO host on addition of $LiClO_4$, which also vary with MMT concentration. However, the *RI* values of SC films have less variation as compared to that of the MP films with increase of MMT concentration. It is expected because large range complexations are formed in the solutions of these electrolytes. Further, from the *RI* values (Tables 2 and 3) it can be concluded that the amorphicity of SC films is higher than that of the MP films. It seems that the electrolyte solutions get more disordered structures under ball milling as compared to the electrolyte composition in dry state blended by same technique. Further, there is no peak corresponding to pure $LiClO_4$ in the XRD patterns of these electrolytes, which indicates the complete dissociation of the salt in the polymeric solutions and also in melt PEO matrix. The confirmation of salt dissociation from the XRD patterns of the solid polymer electrolytes has been subject of several investigations[13,14].

3.2 Complex dielectric spectra

Figures 3 and 4 show the spectra of real part ε' and loss part ε'' of the complex dielectric function $\varepsilon^*(\omega)$ of the ball mill blended SC and MP films of PEO_{20}-$LiClO_4$–*x* wt% MMT electrolytes, respectively. The ε' spectra of these materials have dispersion in the middle frequency region, which is in agreement with the investigations on similar type of SPNE materials[5,12,15,16,29,31]. The ε' values of MMT filled electrolytes are found to be high as compared to that of without MMT. Further, the MP electrolyte films have high ε' values in comparison to that of the SC films. These results infer that the dielectric polarization of the electrolyte having same composition is influenced by their processing (blending) and synthesization techniques. The dielectric relaxation strength $\Delta\varepsilon$, which is a measure of ionic polarization in the ion conducting electrolyte material, was estimated by using their ε' values at 1 kHz (low frequency static permittivity) and 1 MHz (high frequency limiting value), i.e. $\Delta\varepsilon = \varepsilon'(1\text{ kHz}) - \varepsilon'(1\text{ MHz})$, and these values have been presented in Table 4.

Comparative analysis of Figs 3 and 4 confirms that the ε'' values of MP films are high as compared to the

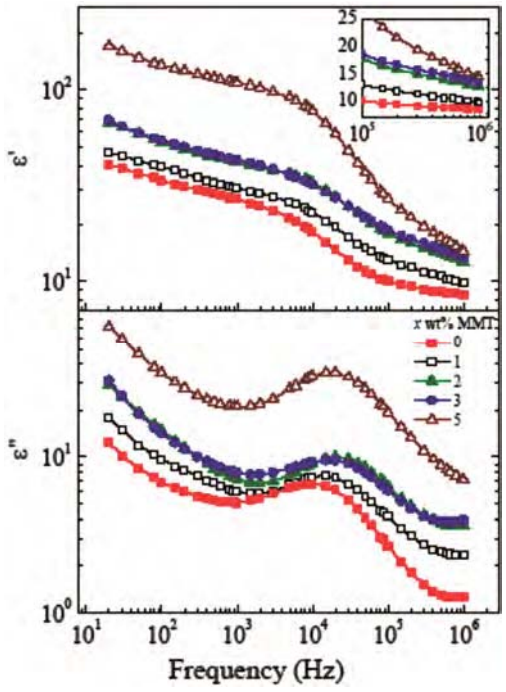

Fig. 3 — Frequency dependent real part ε' and loss ε'' of the complex dielectric function of ball mill blended solution cast PEO_{20}-$LiClO_4$–*x* wt% MMT electrolyte films. Inset shows the high frequency ε' values on linear scale

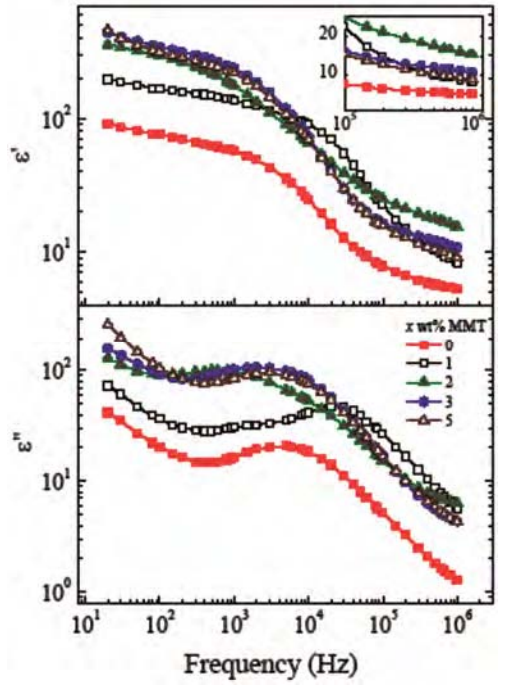

Fig. 4 — Frequency dependent real part ε' and loss ε'' of the complex dielectric function of ball mill blended melt pressed PEO_{20}-$LiClO_4$–*x* wt% MMT electrolyte films. Inset shows the high frequency ε' values on linear scale

Table 4 — Values of real part of permittivity ε' at 1 kHz and 1 MHz, dielectric strength $\Delta\varepsilon = \varepsilon'$ (1 kHz) – ε' (1 MHz), dielectric relaxation time τ_ε, loss tangent relaxation time $\tau_{\tan\delta}$, conductivity relaxation time τ_σ and dc ionic conductivity σ_{dc} of ball mill blended solution cast and melt pressed PEO_{20}–$LiClO_4$–x wt% MMT electrolyte films.

x wt% MMT	ε' at 1 kHz	ε' at 1 MHz	$\Delta\varepsilon$	τ_ε (μs)	$\tau_{\tan\delta}$ (μs)	τ_σ (μs)	$\sigma_{dc}\times10^7$ (S/cm)
Solution cast electrolyte							
0	26.82	8.43	18.39	17.11	7.58	3.46	0.54
1	30.90	9.71	21.19	11.58	5.35	2.24	0.66
2	41.78	12.64	29.14	7.99	3.42	1.47	1.62
3	42.80	13.35	29.45	9.53	4.00	1.64	1.60
5	108.94	14.35	94.59	9.29	2.71	0.10	3.91
Melt pressed electrolyte							
0	57.14	5.30	51.84	34.19	6.18	0.95	2.20
1	137.13	8.32	128.81	7.55	1.58	0.13	13.8
2	175.74	15.28	160.46	254.37	8.88	0.52	4.87
3	235.67	10.83	224.84	81.99	5.36	0.78	6.95
5	218.46	9.03	209.43	53.43	4.85	0.26	6.03

SC films of these electrolytes at same MMT concentration. Further, the MMT filled electrolyte materials have large ε'' values as compared to the electrolyte of without MMT. The ε'' spectra of these materials have the dielectric relaxation peaks in the middle frequency range. The frequency $f_{p(\varepsilon'')}$ corresponding to these peaks was used to determine the dielectric relaxation time τ_ε using the relation[47] $\tau_\varepsilon = 1/2\pi f_{p(\varepsilon'')}$. The evaluated τ_ε values of these electrolytes are recorded in Table 4. These τ_ε values can be assigned to the cations coupled PEO chain segmental dynamics, which mainly governs the ions transportation in these electrolytes through hopping mechanism i.e. the jump of a mobile ion cannot be treated as an isolated event[15].

3.3 AC conductivity spectra

Frequency dependent real part σ′ of *ac* electric conductivity and loss tangent ($\tan\delta = \varepsilon''/\varepsilon'$) of the PEO_{20}-$LiClO_4$–x wt% MMT electrolyte films prepared by SC and MP techniques through ball mill blending are shown in Figs 5 and 6, respectively. These spectra confirm that the σ' values of MMT filled electrolytes are higher than that of the MMT free electrolyte, which mainly results due to formation of intercalated MMT structures in these electrolytes. In most of the MMT filled solid electrolytes, the intercalated MMT structures increase the favourable ion conduction path and hence the ionic conductivity increases[4,37]. It is found that the high frequency σ' spectra of these electrolytes obey the Jonscher's power law[48], whereas a large decrease of σ' values with decrease of frequency in the low frequency region is due to the electrode polarization (EP)

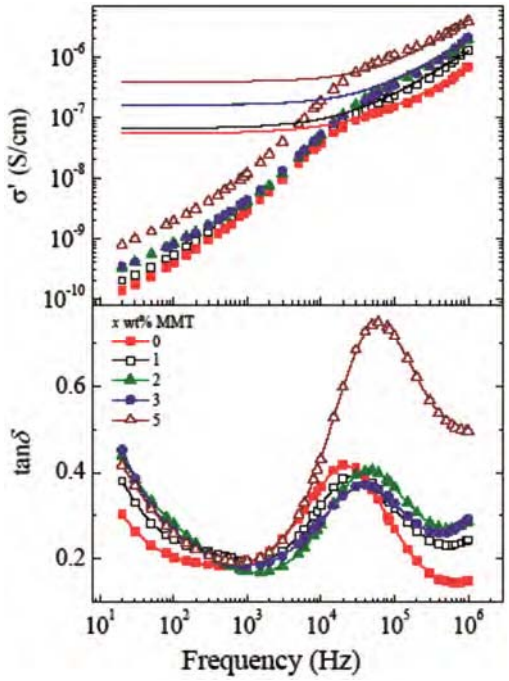

Fig. 5 — Frequency dependent real part σ' of *ac* conductivity and loss tangent $\tan\delta$ of ball mill blended solution cast PEO_{20}-$LiClO_4$–x wt% MMT electrolyte films. The continuous solid line in σ' spectra represent the fit of experimental data to the Jonscher power law $\sigma'(\omega)=\sigma_{dc}+A\omega^n$

effect[29,31,49]. The continuous lines in the σ' spectra of Figs 5 and 6 represent the Jonscher's power law $\sigma'(\omega)=\sigma_{dc}+A\omega^n$ fit to their high frequency experimental values. In power law, σ_{dc} is the *dc* ionic conductivity, A is pre-exponential factor and n is fractional exponent. The evaluated σ_{dc} values of these electrolytes are given in Table 4.

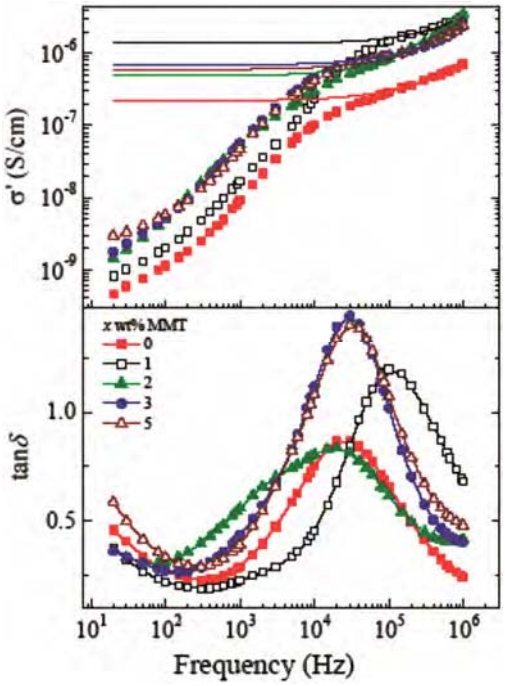

Fig. 6 — Frequency dependent real part σ' of *ac* conductivity and loss tangent tanδ of ball mill blended melt pressed PEO_{20}-$LiClO_4$–*x* wt% MMT electrolyte films. The continuous solid lines in σ' spectra represent the fit of experimental data to the Jonscher power law $\sigma'(\omega)=\sigma_{dc}+A\omega^n$

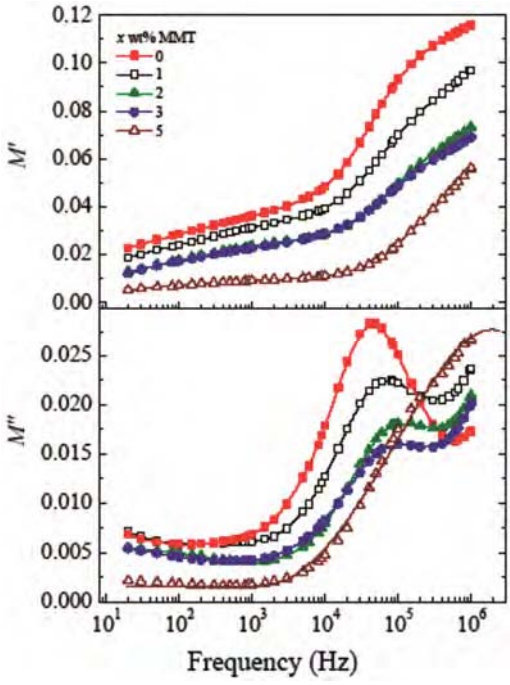

Fig. 7 — Frequency dependent real part M' and loss M'' of complex electric modulus of ball mill blended solution cast PEO_{20}-$LiClO_4$–*x* wt% MMT electrolyte films. Solid line in M'' spectra is the polynomial fit of the experimental data points at 5 wt% concentration

Figures 5 and 6 show that the tanδ spectra of these electrolyte materials have the relaxation peaks in the frequency range ~10^4-10^5 Hz. These peaks are found to be at high frequencies as compared to the values of peaks frequencies in the ε'' spectra of respective MMT concentration electrolyte materials. Using the frequency $f_{p(\tan\delta)}$ values corresponding to tanδ peaks, the loss tangent relaxation time $\tau_{\tan\delta} = 1/2\pi f_{p(\tan\delta)}$ was determined, and these values are recorded in Table 4. Further, it is found that the magnitude of tanδ values of MP films is high as compared to the respective SC films of these electrolyte materials.

3.4 Electric modulus spectra

The electrolyte materials commonly show the ionic conduction relaxation process in their electric modulus $M^*(\omega)$ spectra[13-15,17,29-31,49,50]. This phenomenon is observed both in the solid electrolytes and the liquid electrolytes/dielectrics[51-56]. In $M^*(\omega)$ spectra, the effect of high capacitance phenomena due to space charge effect at low frequencies is automatically suppressed, which is the advantage of this formalism over the dielectric spectra. Figs 7 and 8 show the spectra of real part M' and loss M'' of

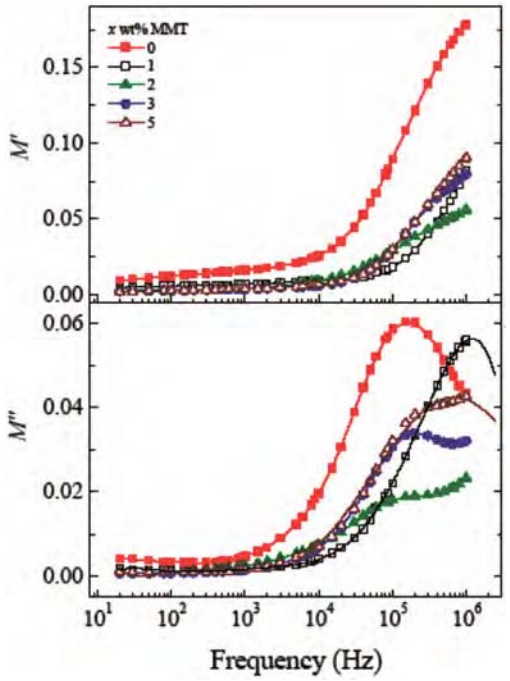

Fig. 8 — Frequency dependent real part M' and loss M'' of complex electric modulus of ball mill blended melt pressed PEO_{20}-$LiClO_4$–*x* wt% MMT electrolyte films. Solid line in M'' spectra is the polynomial fit of the experimental data points at 1 and 5 wt% concentration

electric modulus of ball mill blended SC and MP films of PEO_{20}-$LiClO_4$–x wt% MMT electrolytes, respectively. The M' spectra of these electrolytes have dispersion in high frequency region, whereas these values are relatively very small in the EP affected low frequency region and remain almost frequency independent.

The ionic conductivity relaxation peaks are observed in M'' spectra and these peaks are found at high frequencies as compared to that of the peak frequency values of tanδ spectra of the respective materials, which is found to be in agreement to the earlier investigations[29,31,51]. The change in ions from *dc* to *ac* transport starts at M'' peaks i.e. at frequencies higher than these peak frequencies, the probability for the ion to go back again to its initial site (jumps from one site to its neighbouring vacant site) increases due to the short time periods available. The high probability for correlated forward-backward hopping at high frequencies together with the relaxation of dynamic cage potential are responsible for high frequency σ' dispersion as oberved in Figs. 5 and 6. The most probable ionic conduction relaxation time, τ_σ (also denoted by τ_M) of these materials was estimated by the relation[29] $\tau_\sigma = 1/2\pi f_{p(M)}$, where $f_{p(M)}$ is the frequency corresponding to the M'' peak, and the observed τ_σ values were recorded in Table 4.

3.5 Complex impedance plots

Figures 9 and 10 show Z'' versus Z' plots of SC and MP films of PEO_{20}–$LiClO_4$–x wt% MMT electrolytes, respectively. These plots have arcs at high frequencies (shown in insets) corresponding to bulk conductivity of the materials, which represents the parallel resistance and bulk capacitance of the electrolytes, whereas the spikes at low frequencies represent the EP effect[29,31]. The intercept of high frequency arc and the start of spike on Z' axis gives the values of *dc* resistance of the bulk material, which is commonly used for the evaluation of σ_{dc} values[26,27,57–60]. In the present study, the σ_{dc} values of the electrolyte materials were determined by Jonscher's power law fit to the σ' spectra as discussed in section 3.3, which is more appropriate technique[29,31,49,52–55]. The size of these high frequency arcs is very small and seems to disappear on full frequency range of Z'' and Z' of these electrolytes, which indicates that the current carriers are ions and the total conductivity is mainly the result of ion conduction as concluded earlier for the ion conducting electrolytes[57]. Further, the low frequency spike must be parallel to Z″ axis but the formation of double layer at blocking electrodes results the curvatures in these spikes.

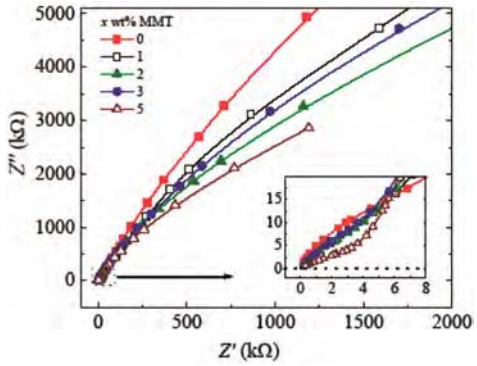

Fig. 9 — Complex impedance plane plots (Z'' versus Z') of ball mill blended solution cast PEO_{20}-$LiClO_4$–x wt% MMT electrolyte films. Inset shows the enlarged view at high frequency data

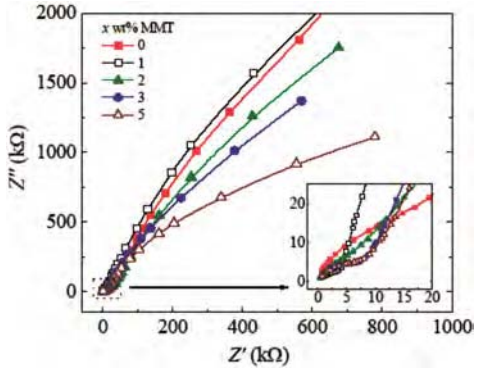

Fig. 10 — Complex impedance plane plots (Z'' versus Z') of ball mill blended melt pressed PEO_{20}-$LiClO_4$–x wt% MMT electrolyte films. Inset shows the enlarged view at high frequency data

3.6 Correlation between ionic conductivity and dielectric parameters

The *dc* ionic conductivity of an ion conducting solid electrolyte material is given by the relation $\sigma_{dc} = \Sigma n_i \mu_i q_i$, where n_i, μ_i and q_i refer to the charge carriers density, free charge (unpaired ions) carriers mobility and the charge of the i^{th} ion (monovalent, divalent, etc), respectively. For a fixed charge ion, the n_i and μ_i values govern the σ_{dc} value of an electrolyte material. For the studied materials, it is found that the σ_{dc} values of MP films of PEO_{20}-$LiClO_4$–x wt% MMT electrolytes are high as compared to that of the respective SC films having same MMT concentration (Table 4). This observation favours that the hot pressing of polymeric electrolyte film results its smooth surfaces which increases the charge density, and also forms some new ion conducting paths favourable to increase the ion conduction mechanism[6,29-32,34-36].

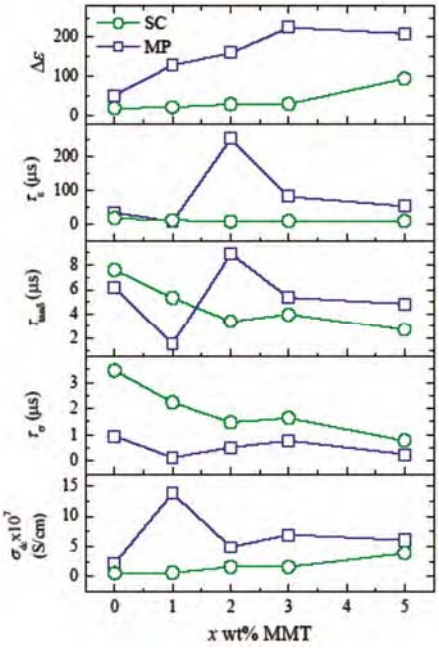

Fig. 11 — MMT concentration dependent dielectric relaxation strength $\Delta\varepsilon$, dielectric relaxation time τ_ε, loss tangent relaxation time $\tau_{\tan\delta}$, conductivity relaxation time τ_σ and dc ionic conductivity σ_{dc} of ball mill blended solution cast (SC) and melt pressed (MP) PEO_{20}-$LiClO_4$–*x* wt% MMT electrolyte films

Figure 11 shows that the σ_{dc} values of ball milled synthesized SC films of SPNEs have gradual increase with the increase of MMT concentration and this increase is nearly 7 times at 5 wt% MMT filler as compared to that of without MMT electrolyte. This increase in σ_{dc} values is slightly lower than that of the earlier investigated similar type of SPNE materials, which were also prepared through high energy ball milling but their milling duration was very high[38,39,41]. The increase of σ_{dc} values with increase of MMT concentration in the electrolytes are also supported by increase of their $\Delta\varepsilon$ values and simultaneously the decrease of the values of various relaxation times (Fig. 11 and Table 4). At fixed concentration of salt in these electrolytes, the enhancement of $\Delta\varepsilon$ values with increase of MMT concentration confirms the increase of ionic polarization, which is due to reduce of ion-pairing effect in the presence of exfoliated MMT nanoplatelets. This results the increase of unpaired ions concentration and the ionic conductivity of these electrolytes. Further, the decrease of relaxation times (τ_ε, $\tau_{\tan\delta}$ and τ_σ) with increase of MMT concentration also confirms the increase of Li^+ cations coupled PEO segmental motion, which increases the ions mobility and results in increase of ionic conductivity of the electrolyte material.

Earlier it has been established that the Li^+ cation has four to six sites of coordination with etheric oxygen molecules of PEO and also the siloxane groups of MMT nanoplatelets, due to which the complexes of these materials form crosslinked transient structures in dynamical state and promote the cations transportation[21,31,61,62]. Besides this fact, the MMT platelets also coordinate with anions and reduce the ion-pairing effect, and hence increase the ionic conductivity. Furthermore, the amorphous phase of the electrolyte also plays an important role in the enhancement of its ionic conductivity[4,13,14,49,58]. Table 2 presents that the *RI* values of MMT filled electrolytes are lower than that of MMT free electrolyte, which reveals that the presence of MMT increases the amorphous phase of the electrolyte and favours the increase of ions mobility due to increase of local free volume in the amorphous phase of material. Besides these facts, the formation of intercalated MMT structures, as evidenced from the increase of d_{001} spacing, also favours the increases of σ_{dc} values of these SC electrolytes, because earlier it has been established that the intercalated MMT connects the favourable ion conductive paths in the MMT filled SPNE materials[4,49,58]. Therefore, from the comparative dielectric parameters and the *RI* values, it can be concluded that the enhancement in σ_{dc} value with the increase of MMT filler in SC films of PEO_{20}-$LiClO_4$–*x* wt% MMT electrolytes may be due to combined effects of the increase in amount of salt dissociation, reduce of ion-pairing effect, increase of nanometric channels and their connectivity with cations mobility, the increase of PEO amorphous phase and also the increase of PEO chain segmental dynamics.

Figure 11 shows that the σ_{dc} values of ball milled blended MP films of PEO_{20}-$LiClO_4$–*x* wt% MMT electrolytes have maximum increase at 1 wt% MMT, which is nearly 6 times high as compared to that of without MMT electrolyte (Table 4). This increase is favoured by a large increase of its $\Delta\varepsilon$ value and also a significant decrease of $\tau_{\tan\delta}$ value. Although the $\Delta\varepsilon$ values also have an increase at 2 and 3 wt% MMT but the comparative high relaxation times values at these concentrations are the reasons for their low σ_{dc} values as compared to that of the 1 wt% MMT filled solid electrolyte. At 5 wt% MMT electrolyte, the $\Delta\varepsilon$ has a decrease (Table 4) but its relaxation times values are close to 3 wt% MMT filled electrolyte, so the σ_{dc} has a small decrease at this concentration. The comparative *RI* values of these electrolytes (Table 3)

also favour the changes in the σ_{dc} values with MMT concentration. As compared to the σ_{dc} values of agate mortar and pestle blended and melt pressed synthesized PEO_{20}-$LiClO_4$–*x* wt% MMT electrolyte films[31], the ball mill blended melt pressed electrolytes of same composition have relative high ionic conductivity. Further, in such electrolytes, the bulky anions (ClO_4^-) exist somewhere in the polymer backbone or coordinate with surface of MMT and has insignificant contribution in the ionic conductivity[29,31], and the ionic conduction is mainly due to cations transportation. Furthermore, although the amorphicity of SC films are high as compared to MP films but the ionic conductivity of MP films is high. This suggests that the other factors (dielectric strength, relaxation time and MMT intercalated structures) mask the crystallinity effect on ionic conductivity of MP electrolyte films.

4 Conclusions

The XRD study of ball mill blended synthesized SC and MP films of PEO_{20}-$LiClO_4$–*x* wt% MMT electrolytes confirms the complex formation between oxygen atoms of PEO, Li^+ cations and the siloxane groups of exfoliated MMT nanoplatelets, which results in the increase of their amorphous phase. These materials also form intercalated MMT structures and the amount of intercalation increases with increase of MMT concentration. The MP electrolyte films have high ionic conductivity (maximum at 1 wt% MMT) as compared to that of SC electrolyte films. The ionic conductivity of SC films increases 7 times with increase of MMT concentration up to 5 wt%. A correlation is observed between the ionic conductivity and dielectric parameters (dielectric relaxation strength and relaxation times) of these electrolyte materials, which is also supported by their amorphicity. The melt pressed synthesized polymeric electrolytes have increase of surface charge density which increases their ionic conductivity as compared to the solution cast electrolyte films. The dielectric parameters mask the crystallinity effect on the ionic conductivity of MP electrolyte films.

Acknowledgement

Authors are grateful to the Department of Science & Technology (DST), New Delhi for providing the experimental facilities through research projects Nos. SR/S2/CMP-09/2002, SR/S2/CMP-0072/2010 and the DST–FIST program. One of the authors SC is thankful to the CSIR, New Delhi for the award of Research Associate fellowship.

References

1 Scrosati B & Garche J, *J Power Sources*, 195 (2010) 2419.
2 Sharma P, Kanchan D K, Gondaliya N, Jayswal M & Joge P, *Indian J Pure & Appl Phys*, 51 (2013) 346.
3 Kumar Y, Hashmi S A & Pandey G P, *Solid State Ionics*, 201 (2011) 73.
4 Mohapatra S R, Thakur A K & Choudhary R N P, *J Power* Sources, 191 (2009) 601.
5 Karan N K, Pradhan D K, Thomas R, Natesan B & Katiyar R S, *Solid State Ionics*, 179 (2008) 689.
6 Zhou X, Yin Y, Wang Z, Zhou J, Huang H, Mansour A N, Zaykoski J A, Fedderly J J & Balizer E, *Solid State Ionics*, 196 (2011) 18.
7 Deka M & Kumar A, *Electrochim Acta*, 55 (2010) 1836.
8 Sharma A L & Thakur A K, *Ionics*, 16 (2010) 339.
9 Johan M R, Shy O H, Ibrahim S, Yassin S M M & Hui T Y, *Solid State Ionics*, 196 (2011) 41.
10 Köster T K J & van Wüllen L, *Solid State Ionics*, 181 (2010) 489.
11 Ulaganathan M & Rajendran S, *Ionics*, 16 (2010) 667.
12 Munar A, Andrio A, Iserte R & Compañ V, *J Non-Cryst Solids*, 357 (2011) 3064.
13 Ravi M, Pavani Y, Kiran Kumar K, Bhavani S, Sharma A K & Narsimha Rao V V R, *Mater Chem Phys*, 130 (2011) 442.
14 Kiran Kumar K, Ravi M, Pavani Y, Bhavani S, Sharma A K & Narsimha Rao V V R, *J Non-Cryst Solids*, 358 (2012) 3205.
15 Karmakar A & Ghosh A, *J Appl Phys*, 107 (2010) 104113 (pp 6).
16 Karmakar A & Ghash A, *Current Appl Phys*, 12 (2012) 539.
17 Ramesh S, Shanti R & Durairaj R, *J Non-Cryst Solids*, 357 (2011) 1357.
18 Deka M & Kumar A, *J Solid State Electrochem*, 14 (2010) 1649.
19 Pandey G P, Agrawal R C & Hashmi S A, *J Solid State Electrochem*, 15:2253–2264.
20 Vickraman P, Aravindan V & Lee Y S, *Ionics*, 16 (2010) 263.
21 Zhang J, Huang X, Wei H, Fu J, Huang Y & Tang X, *J Solid State Electrochem,* 16 (2012) 101.
22 Tripathi S K, Gupta A, Jain A & Kumari M, *Indian J Pure & Appl Phys*, 51 (2013) 358.
23 Fan L, Dang Z, Wei G, Nan C W & Li M, *Mater Sci Eng B*, 99 (2003) 340.
24 Ramesh S & Chai M F, *Mater Sci Eng B*, 139 (2007) 240.
25 Wang L, Yang W, Wang J & Evans D G, *Solid State Ionics*, 180 (2009) 392.
26 Marzantowicz M, Dygas J R & Krok J, *Electrochim Acta*, 53 (2008) 7417.
27 Kim S, Hwang E J, Jung Y, Han M & Park S J, *Colloids Surf A: Physicochem Eng Aspects*, 313-314 (2008) 216.
28 Ramesh S & Liew C W, *J Non-Cryst Solids*, 358 (2012) 931.
29 Sengwa R J, Sankhla S & Choudhary S, *Ionics,* 16 (2010) 697.
30 Choudhary S & Sengwa R J, *Indian J Pure & Appl Phys,* 49 (2011) 600.
31 Choudhary S & Sengwa R J, *Ionics,* 17 (2011) 811.
32 Choudhary S & Sengwa R J, *Ionics,* 18 (2012) 379.
33 Appetecchi G B, Croce F, Hassoun J, Scrosati B, Salomon M & Cassel F, *J Power Sources,* 114 (2003) 105.
34 Chandra A, Chandra A & Thakur K, *Indian J Pure & Appl Phys,* 51 (2013) 44.

35 Pandey G P, Hashmi S A & Agarwal R C, *Solid State Ionics,* 179 (2008) 543.
36 Agrawal R C, Mahipal Y K & Ashrafi R, *Solid State Ionics*, 192 (2011) 6.
37 Aranda P, Mosqueda Y, Pérez-Cappe E & Ruiz-Hitzky E, *J Polym Sci Part B: Polym Phys,* 41 (2003) 3249.
38 Shin J H, Lim Y T, Kim K W, Ahn H J & Ahn J H, *J Power Sources,* 107 (2002) 103.
39 Shin J H, Kim K W, Ahn H J & Ahn J H, *Mater Sci Eng B,* 95 (2002) 148.
40 Patel P, Kim I & Kumta P N, *Mater Sci Eng B,* 116 (2005) 347.
41 Shin J H, Jung B S, Jeong S S, Kim K W, Ahn H J, Cho K K & Ahn J H, *Metals Mater,* 10 (2004) 177.
42 Sengwa R J, Choudhary S & Sankhla S, *Compos Sci Technol*, 70 (2010) 1621.
43 Homminga D, Goderis B, Dolbnya I, Reynaers H & Groeninckx G, *Polymer,* 46 (2005) 11359.
44 Sapalidis A A, Katsaros F K, Steriotis ThA & Kanellopoulos N K, *J Appl Polym Sci,* 123 (2012) 1812.
45 Shukla N & Thakur A K, *Ionics,* 15 (2009) 357.
46 Hodge R M, Edward G H & Simon G P, *Polymer,* 37 (1996) 1371.
47 Choudhary S & Sengwa R J, *J Appl Polym Sci,* 124 (2012) 4847.
48 Jonscher A K, *Dielectric Relaxation in Solids*. Chelsea Dielectric Press, London (1983).
49 Pradhan D K, Choudhary R N P & Samantaray B K, *Mater Chem Phys,* 115 (2009) 557.
50 Sharma P, Kanchan D K, Gondaliya N, Pant M & Jayswal M S, *Ionics,* 19 (2013) 301.
51 Zhang S, Dou S, Colby R H & Runt J, *J Non-Cryst Solids,* 351 (2005) 2825.
52 Sengwa R J, Choudhary S & Sankhla S, *Polym Int,* 58 (2009) 781.
53 Sengwa R J, Choudhary S & Sankhla S, *Colloids Surf A: Physicochem Eng Aspects,* 336 (2009) 79.
54 Sengwa R J, Sankhla S & Choudhary S, *Colloid Polym Sci,* 287 (2009) 1013.
55 Choudhary S & Sengwa R J, *Indian J Eng Mater Sci,* 18 (2011) 147.
56 Choudhary S & Sengwa R J, *Indian J Phys,* 86 (2012) 335.
57 Malathi J, Kumaravadivel M, Brahmanandhan G M, Hema H, Baskaran R & Selvasekarapandian S, *J Non-Cryst Solids,* 356 (2010) 2277.
58 Pradhan D K, Choudhary R N P, Samantaray B K, Thakur A K & Katiyar R S, *Ionics,* 15 (2009) 345.
59 Qian X, Gu N, Cheng Z, Yang X, Wang E & Dong S, *J Solid State Electrochem,* 6 (2001) 8.
60 Ravi M, Bhavani S, Pavani Y & Narasimha Rao V V R, *Indian J Pure & Appl Phys*, 51 (2013) 362.
61 Chen H W & Chang F C, *Polymer,* 42 (2001) 9763.
62 Choudhary S & Sengwa R J, *Indian J Pure & Appl Phys,* 49 (2011) 204.